Self-invertible 2D log-Gabor wavelets

Sylvain Fischer[a,b], Filip Šroubek[a,c], Laurent Perrinet[b], Rafael Redondo[a], Gabriel Cristóbal[a]
[a]Instituto de Optica, CSIC, Serrano 121, 28006 Madrid, Spain
[b]INCM, UMR6193, CNRS & Aix-Marseille University, 31 ch. Aiguier, 13402 Marseille Cedex 20, France
[c]Academy of Sciences, Pod vodárenskou věží 4 Prague, Czech Republic

***Abstract*— Biorthogonal wavelets got a very popular image processing tool but exhibit major drawbacks, namely a poor resolution in orientation and the lack of translation invariance due to the aliasing between subbands. Alternative multiresolution transforms which specifically solve these drawbacks have been proposed. These transforms are generally overcomplete and consequently offer huge degrees of freedom in their design. At the same time their optimization gets a challenging task. We proposed here a log-Gabor wavelet transform gathering the excellent mathematical properties of the Gabor functions with a carefully construction to maintain the properties of the filters and to permit exact reconstruction. Two major improvements are proposed: first the highest frequency bands are covered by narrowly localized oriented filters. And second, all the frequency bands including the highest and lowest frequencies are uniformly covered and thus exact reconstruction is achieved using the same filters in both the direct and the inverse transforms (which means that the transform is self-invertible). The transform is optimized not only mathematically but it also follows as much as possible the knowledge on the receptive field of the simple cells of the Primary Visual Cortex (V1) of primates and on the statistics of natural images. Compared to the state of the art, the log-Gabor wavelets show excellent behavior in their ability to segregate the image information (e.g. the contrast edges) from incoherent Gaussian noise by hard thresholding and to code the image features through a reduced set of coefficients with large magnitude. Such characteristics make the transform a promising tool for general image processing tasks.**

***Index Terms*— wavelet transforms, log-Gabor filters, oriented high-pass filters, image denoising, visual system.**

I. Introduction

After the development and rapid successes of the wavelets transforms in image processing, alternative multiresolutions have been proposed mainly for a better resolution in orientation and for avoiding aliasing effects. Last fifteen years oriented band-pass multiresolution transforms have arisen with increased importance thanks to the development of steerable pyramids [1], Gabor multiresolution [2], [3], [4], complex-valued wavelets [5], [6], curvelets [7] and contourlets [8], to name a few.

A Gabor function is a Gaussian multiplicated by a complex exponential. Thus, in the Fourier domain, it is a Gaussian shifted from the origin. Gabor functions gather a number of interesting mathematical properties: first they have a smooth and infinitely differentiable shape. Second, their modulus are monomodal, i.e. they have no side lobes neither in space nor in Fourier. Third, they provide an optimum joint localization in space and frequency [9]. For such good properties they have been proposed as ideal functions for signal processing. Similarly, 2D Gabor functions are highly jointly selective to a specific position, orientation and spatial frequency. Neuroscience studies have shown that the receptive fields of simple cells of the Primary Visual Cortex (V1) of primates can be modelled by Gabor functions [10], [11]. Considering natural vision as optimized by the millions of years of evolutionary pressure, the recruitment of Gabor functions by V1 can be seen as an additional argument in favor of their adequacy for image processing.

Nevertheless Gabor functions present some important drawbacks. They are not orthogonal, which prevents to build an orthogonal basis of decomposition. Non-orthogonality implies that exact reconstruction using the same filters for analysis and synthesis will not be possible unless an overcomplete basis is considered. Moreover Gabors are bandpass filters, they are consequently inadequate for covering the lowest and highest frequencies. Additionally it is particularly difficult to cover up the mid frequencies with sufficient uniformity. Nevertheless they have successfully been used for image analysis and applications where exact reconstruction is not required, such as texture analysis [12], [4], texture synthesis [13], edge/contour extraction [14], [15], [16], object recognition [17], [18]. And, even without exact reconstruction they have been shown useful for image restoration applications [19], [20], [21], [22]. In parallel, different methods for reconstruction improvement have been proposed to recover the highest frequencies [3], to avoid excessive low-pass overlapping [23], to improve the reconstruction [24], [25] or to cover more uniformly the Fourier domain [2].

One of the important applications where oriented multiresolution schemes appeared to be particularly efficient is image denoising. In this field bi-orthogonal wavelets are themselves one of the most popular and optimal tool [26]. Nevertheless it has been shown that undecimated wavelets provide better results than the classical critically sampled wavelets [27], [28], [29]. Latter works have shown the interest of redesigning the Fourier domain tiling, particularly for increasing the number of orientations [7], [8], [30]. Indeed the relaxation of the critical sampling constraint provides high degrees of freedom in the construction of the multiresolution scheme and it is worth taking advantage of this additional flexibility for choosing the filter shape, the bandwidths, the degree of overlapping between filters, the number of orientations, or for choosing complex-valued filters, etc. We propose in this paper a transform

This work has been supported in part by the grants TEC 2004-00834, PI040765, and the G03/185, TEC2005-24738-E thematic networks. SF and RR are supported by MEC-FPU and CSIC-I3P fellowships, respectively. LP is supported by a grant from the CNRS - ACI "Temps & cerveau".

optimized following mathematical, biological, perceptual and natural image statistics criteria. The rationale for taking into account those additional criteria besides the mathematical ones is: (1) the number of free parameters is prohibitive for a systematic study. (2) The Primary Visual Cortex supposedly evolved towards an efficient and robust image processing system adapted to natural images. Considering the important similarity between V1 simple cells and oriented multiresolution transforms, we hypothesize that biological knowledge on V1 could serve as an useful guide for the choice of the free parameters. Moreover as an interesting feedback the implementation of biologically inspired wavelet transforms could help to improve the understanding of V1. (3) It is important to provide good image quality from the human perceptual point of view, since digital images are almost exclusively used by humans. It is then to construct methods limiting the appearance of perceptually salient artefacts. The similarity with the biological models can help for such an objective. (4) The multiresolution must be built according to the type of signal to analyze. Here as we focus on natural images, studies on their statistics can also be used as guidelines. Moreover it is worth noting that there are direct relationships between receptive fields of V1 and statistics of natural images [23], [31], [32].

We propose then here an implementation of a multiresolution transform following these constraints: (1) an optimal localization in space, frequency and orientation through the use of Gabor filters; (2) an augmented number of orientations; (3) a resemblance to the receptive field of V1 simple cells; (4) an exact reconstruction by a self-invertible transform (the same transform functions are used for the direct and inverse transforms) and (5) complex-valued filters sensible to both symmetric and antisymmetric features. We pay special attention to the different aspects of the design of the multiresolution scheme and we propose a series of solutions for improving the efficiency of the Gabor wavelets scheme. In comparison with previous implementations of Gabor multiresolution ([2], [3], [4], [13]), the most important novelties of the present work consists in incorporating complex-valued oriented high-pass filters, and achieving the exact reconstruction (self invertibility) property.

The present paper fulfills two objectives: first to describe in detail in the Section II the proposed self-invertible log-Gabor transform which we already employed successfully in a variety of applications such as denoising [33], [34], edge extraction [33], compression [35], [36], image fusion [37], but whose implementation was incomplete or not described in detail in those papers. Second to illustrate (in Section III) the efficiency of the method in an image denoising scenario. Finally, we conclude in Section IV.

II. Method

Let's consider a $n \times n$ square image $\mathbf{x}$ of $N = n^2$ pixels. The Gabor wavelets $\mathcal{W}$ consist in filtering the input image $\mathbf{x} \in \mathbb{R}^N$ by a set of filters $(\mathbf{G}_r)_{r \in \Omega}$. The band-pass, high-pass and low-pass filters are described respectively in Sections II-A, II-B and II-C. Direct and inverse transforms are defined in Sections II-D and II-E, respectively. Section II-F describes the downsampling method and Section II-G deals with the matrix notation. Methods for obtaining exact reconstruction are listed in Section II-H.

A. Bandpass log-Gabor filters

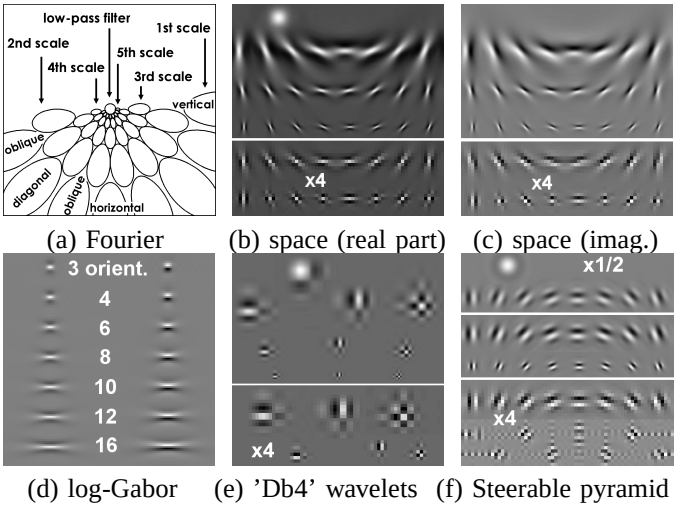

(a) Fourier (b) space (real part) (c) space (imag.)

(d) log-Gabor (e) 'Db4' wavelets (f) Steerable pyramid

Fig. 1. Multiresolution schemes. **a.** Schematic contours of the log-Gabor filters in the Fourier domain with 5 scales and 8 orientations (only the contours at 78% of the filter maximum are drawn). **b.** Real part of the corresponding filters in the spatial domain. The two first scales are drawn at the bottom magnified by a factor of 4 for a better visualization. The different scales are arranged in lines and the orientations in columns. The low-pass filter is drawn in the upper-left part. **c.** The corresponding imaginary part of the filters is shown in the same arrangement. Note that the low-pass filter does not have imaginary part. Insets (b) and (c) show the final filters built through all the processes described in Section II. **d.** The elongation of log-Gabor wavelets increases with the number of orientations n_t (and inversely decreases with the bandwidth in orientation σ_θ). Here the real (left column) and imaginary (right column) parts for 3, 4, 6, 8, 10, 12 and 16 orientations are drawn. **e.** As a comparison biorthogonal wavelets filters 'Db4' are shown. Horizontal, vertical and diagonal wavelets are arranged on columns. **f.** As a second comparison, steerable pyramid filters [30] are shown. The arrangement over scales and orientations is similar to the log-Gabor one. Among differences, the shape is more round while log-Gabor are more elongated, and the filters have no symmetric part. The raised cosine shape in Fourier can induce a less regular shape in the spatial domain (presence of extra side lobes) than with log-Gabor filters. The first scale filters are not closely localized and side lobes appear up to a large distance. Such insufficient localization is overcome in the log-Gabor implementation by procedures described in Section II-B.

Classical Gabor filters give rise to important difficulties when implemented in multiresolution. Filters overlap more importantly in the low frequencies than in the higher ones yielding a non-uniform coverage of the Fourier domain. Moreover Gabor filters are not zero mean, they are then affected by DC components. For those reasons log-Gabor filters are used in the present implementation instead for Gabor filters. The log-Gabor filters lack DC components and can yield a fairly uniform coverage of the frequency domain in an octave scale multiresolution scheme [23]. The log-Gabor filters are defined in the log-polar coordinates of the Fourier domain as Gaussians shifted from the origin:

$$\mathbf{G}_{(s,t)}(\rho,\theta) = \exp\left(-\frac{1}{2}\left(\frac{\rho-\rho_s}{\sigma_\rho}\right)^2\right)\exp\left(-\frac{1}{2}\left(\frac{\theta-\theta_{(s,t)}}{\sigma_\theta}\right)^2\right)$$
$$with \quad \begin{cases} \rho_s = \log_2(n) - s \\ \theta_{(s,t)} = \begin{cases} \frac{\pi}{n_t}t & if\ s\ is\ odd \\ \frac{\pi}{n_t}(t+\frac{1}{2}) & if\ s\ is\ even \end{cases} \\ (\sigma_\rho,\sigma_\theta) = 0.996(\sqrt{\frac{2}{3}},\frac{1}{\sqrt{2}}\frac{\pi}{n_t}) \end{cases} \tag{1}$$

where (ρ,θ) are the log-polar coordinates (in log_2 scale, indicating the filters are organized in octave scales); $n_s = 5$ is the number of scales of the multiresolution scheme and n_t is the number of orientations (n_t will range between 3 to 20, 8 orientations being a typical value). $s \in \{1,..,n_s\}$ and $t \in \{1,..,n_t\}$ index respectively the scale and the orientation of the filter; $(\rho_s,\theta_{(s,t)})$ are the coordinates of the center of the filter; and $(\sigma_\rho,\sigma_\theta)$ are the bandwidths in ρ and θ, common for all filters.

It is highly justified to consider the Fourier domain through the log-polar coordinates. Indeed in such coordinate system, the octave distribution of filters constitutes a regular grid, the center of the filters defined by Eq. 1 laying on an uniform hexagonal lattice. Moreover in such coordinates the filters are purely Gaussian and their bandwidth is a constant independent of the orientation and the scale.

Defined by Eq. 1 the filters cover only one side of the Fourier domain (see also Fig 1.a). It is worth considering them in Fourier as the sum of a symmetric and an antisymmetric components. The components sum their amplitude in one side of the Fourier domain and cancel themselves in the other side. This explains that in the spatial domain, the filters have both a real part (with cosine shape due to the symmetric component) and an imaginary part (with sine shape due to the antisymmetric component). A single log-Gabor filter defined in Fourier by Eq. 1 yields then both a real and an imaginary part in the spatial domain. Both parts can be seen respectively in Fig. 1.b and c for the 5 scales and 8 orientations scheme. They can be compared with the filters used in other decomposition functions (biorthogonal wavelets 'Db4' in Fig. 1.e and steerable pyramids [30] in Fig. 1.f).

One objective of this study is to choose the transform parameters as close as possible of the known physiology of simple cortical cells. Complex log-Gabor filters are chosen for modeling the receptive field of the simple cortical cells as proposed in [10], [11], [23]. Simple cells are known to be organized in pairs in quadrature of phase [38], justifying the choice of complex-valued filters. The choice of the bandwidth in orientation is motivated by the simple cells orientation sensitivity which has been evaluated as around 20-40 degrees of full bandwidth at half response [39], [10]. Such orientation bandwidth would require around 6 to 13 orientations to cover the 180 degrees of the plane. For the proposed scheme using the typical value of 8 orientations we obtain filters with 31.8 degree full bandwidth at half response. The bandwidth in scale of the simple cells has been evaluated between 0.6 and 3.2 octaves [40], and around 1.3 octaves in mean [10] (at half response). The present filters have a 1.43 octave bandwidth. De Valois and al. [40] reported the existence of cells covering different scales over at least 4 octaves for each retina location. At least 3 scales for each retina location have been encountered. This is consistent with the choice of a multi-scale transform. Additionally the shape of the filters shown Fig. 1.b,c appears close to the independent components learned by sparse coding or ICA techniques on natural images [31], [32], confirming the adequacy of the scheme to match image features. By its parts the modulus operation on real and imaginary parts which will be exploited for denoising in Section III induces an independency toward phase which is characteristic of complex cortical cells.

B. High-pass oriented filters

One important problem appear in the first scales where from Eq. 1, $\mathbf{G}_r$ would have significant amplitude above the Nyquist frequency ($\rho \geq log_2(\frac{n}{2})$). Cutting off abruptly the filters above the Nyquist frequency strongly distorts the filter shape in the spatial domain (i.e. causes the appearance of side lobes and ringing). For this reason in many implementations high frequencies are not covered, e.g. in [4]. Alternatively, to not loose this part of the spectrum Nestares and coworkers included a non-oriented high-pass filter [3]. Nevertheless when it is used in denoising or compression, a non-oriented high-pass filter introduces cross-shaped artifacts, which are very salient and artificial-looking. We propose here several solutions to design high-pass filters sensitive to orientation and having smooth shape without extra side lobes. They consist first in incorporating an half-pixel shift in the spatial position of the imaginary part of the filters. This shift allows the first scale filters to capture much more adequately the antisymmetric features, as it will be illustrated Section II-B.3, but consequently the real and imaginary parts have to be separately defined. Also oblique filters are designed in a different way than vertical and horizontal filters ones (Section II-B.1 and 2). Note that, because the definition of the first scale filters differs from the other scales, the transform is no more strictly a "wavelets" one, but it can be considered as a wavelet-like transform since the general shape of the basis functions is obtained by translation, dilatation, and rotation of a mother function if we except the modifications here proposed for improving the reconstruction performances. Moreover the proposed Gabor wavelets build directly on the original Morlet and coworkers proposition of using Gabor functions as a cycle octave multiresolution [41].

1) Real part of the horizontal and vertical filters: The real part of horizontal and vertical filters is defined symmetrically as shown in Fig. 2. Thus they are continuous across the periodicities of the Fourier domain (strong discontinuities in the Fourier domain create side lobes in the spatial domain) and are smooth and without extra side lobes in the space domain.

2) Real part of the diagonal/oblique filters: The real part of non vertical nor horizontal filters is also defined symmetrically. But this is not sufficient to maintain the Fourier domain continuous (across periods) and to keep a good localization in the space domain. We propose then to fold those filters by considering them as periodic with periodicity n. Nevertheless the part higher to the Nyquist frequency ($|u| \geq \frac{n}{2}$ or $|v| \geq \frac{n}{2}$, where (u,v) are the cartesian coordinates of

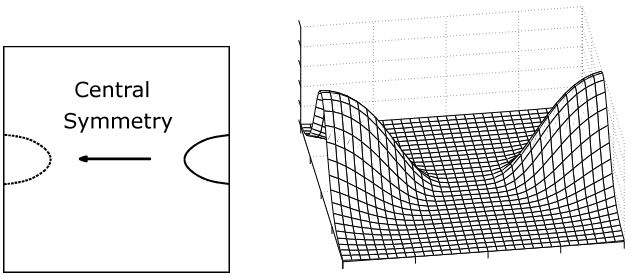

(a) (b)

Fig. 2. The real part of the first scale vertical filter is constructed in Fourier by symmetry. **a.** Contours of the filters in the Fourier domain at 78% of the filter maximum. The filter is build up by summing its central symmetry. **b.** Resulting filter. This filter is shown in spatial domain in Fig. 1.b bottom row, left column.

the Fourier domain) once folded cover the whole spectrum with significant amplitude. To maintain the filter selectivity to high-frequencies, it is then necessary to filter down the induced lowest frequencies by multiplying the folded part by an attenuation function α defined as a raised cosine (see also Fig. 3 for an illustration of the construction of such filters):

$$\alpha = \begin{cases} \frac{1}{2}cos(\pi \frac{d}{n/3}) + \frac{1}{2} & if\ d < n/3 \\ 0 & if\ d > n/3 \end{cases} \quad (2)$$

where d is the distance to the closest frequency inside the Nyquist range (i.e. u and v within $[-n/2, n/2]$).

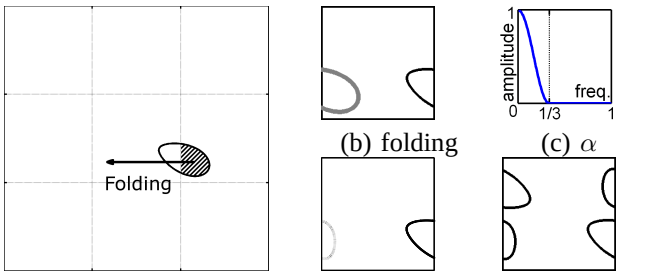

(a) 3× oversampled filter (b) folding (c) α (d) attenuation (e) symmetry

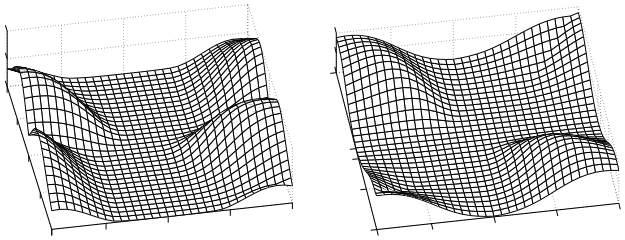

(f) oblique filter (g) diagonal filter

Fig. 3. Construction of diagonal and oblique first scale filters. **a.** The frequency domain is oversampled 3 times. **b.** The frequencies above the Nyquist frequency are folded by periodicity. **c.** Raised cosine function α. **d.** The folded part of the filter is attenuated by multiplication by the raised cosine α. **e.** The central symmetry is summed for the construction of a real-valued filter. **f.** Resulting oblique filter. **g.** Resulting diagonal filter. These filters are shown in the spatial domain in Fig. 1.b bottom row.

3) Imaginary part of the horizontal and vertical filters: The imaginary part is build similarly to the real part (Section II-B.1) but antisymmetrically instead of symmetrically. Moreover the filter must not be centered in the pixels but in the interval between two pixels for two related reasons. First, in the spatial domain, an antisymmetric filter would have a zero as central coefficient, which induces the filter to be almost null in its central part if it has a two pixel period (that is a frequency close to the Nyquist frequency as it is the case here). The filter would then be very coarsely localized, having most of its amplitude far from its center. The filter must then be centered between two pixels (see Fig. 4.a). Second, in the Fourier domain, an antisymmetric high-pass filter is not continuous across periods while a half-pixel shifted version is (see Fig. 4.b). For those reasons the filter is multiplied by a $e^{i\pi\frac{u}{n}}$ or $e^{i\pi\frac{v}{n}}$ function in the Fourier domain (for horizontal and vertical filters, respectively) which induces a half pixel displacement in the space domain. As a consequence the Fourier coefficients are now complex-valued and both the real and imaginary Fourier parts of the filters become continuous across periods (see Fig. 4.b).

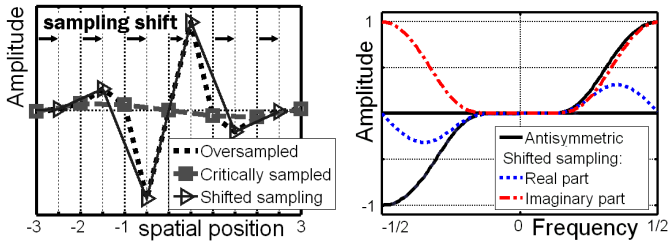

(a) spatial domain (b) Fourier domain

Fig. 4. Imaginary part construction of horizontal and vertical first scale filters. **a.** In the spatial domain it is necessary to shift the sampling grid by half a pixel. A non-shifted sampling yields a function almost null in the central coefficients, most of the amplitude being localized far from the center inducing a very poor localization of the filter. The same antisymmetric filter built on a half-pixel shifted grid is much more closely localized. **b.** Shifting the sampling grid is realized by multiplying the frequencies by $e^{i\pi\frac{u}{n}}$ (inducing the filter coefficients are complex-valued also in the Fourier domain). It makes the filter continuous in its frequency coverage across periods.

4) Imaginary part of non horizontal nor vertical filters: Those filters are defined antisymmetrically and are folded by periodicity with the same attenuation function α described in Section II-B.2. Moreover they are also shifted half the inter-pixel distance perpendicularly to the direction of the filter by multiplication in Fourier by $e^{\frac{i\pi}{n}(u\cdot t_u + v\cdot t_v)\cdot max(|t_u|,|t_v|)}$, where (t_u, t_v) is the normalized direction vector of the channel.

5) Second scale filters: Second scale filters are also folded by periodicity with attenuation α (see Section II-B.2). Here nevertheless they are not separated in symmetrical and antisymmetrical filters and the same definition is used for all orientations. An example of second scale filter is shown in Fig. 5.

C. Low-pass filter

The multiresolution scheme is completed with a low-pass filter for recovering the luminance information. The low-pass filters could be defined simply as a Gaussian low-pass filter as in [13]. Nevertheless for a better filling in of the low-pass residual frequencies not covered by the log-Gabor filters, it is defined in a different way: two additional scales above the number of scale deployed n_s are built and summed up together

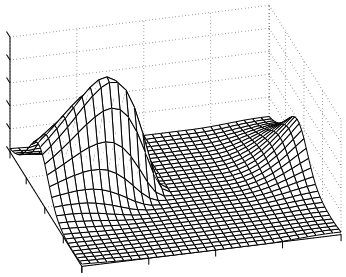

Fig. 5. Second scale filters are constructed in Fourier by folding the filters by periodicity and applying the attenuation function α on the folded part.

(as the root sum squared). Moreover the part inside the highest additional scale is set up to one. In practice if 5 scales are deployed, the filters that would correspond to the 6th and 7th scales are summed and additionally the space inside the 7th scale ($\rho < log_2 n - 7$) is set up to one.

D. Direct log-Gabor wavelet transform

The whole set of bandpass filters, high-pass filters and the low-pass filter are indexed by $\Omega = \{1, .., n_s n_t + 1\}$. The filter set is then refereed as $(\mathbf{G}_r)_{r\in\Omega}$. The convolution of the image $\mathbf{x}$ by a filter $\mathbf{G}_r$ is $\mathbf{h}_r$ which is called a *channel*. It is computed in the Fourier domain as:

$$\mathbf{h}_r = \mathcal{F}^{-1}\left(\mathbf{G}_r \cdot \mathcal{F}(\mathbf{x})\right) \tag{3}$$

where $\mathcal{F}$ and $\mathcal{F}^{-1}$ are respectively the direct and inverse discrete Fourier transform. The Gabor wavelets transform of $\mathbf{x}$ is defined by:

$$\mathcal{W}(\mathbf{x}) = (\mathbf{h}_r)_{r\in\Omega}. \tag{4}$$

Any element of the transform domain, e.g. $(\mathbf{h}_r)_{r\in\Omega}$, is called a *pyramid*.

E. Reconstruction

The reconstruction transform $\mathcal{W}^\dagger$ consists in filtering in Fourier each channel $\mathbf{h}_r$ by the corresponding filter $\overline{\mathbf{G}_r}$ (where $\overline{\mathbf{G}_r}$ is the complex conjugate of $\mathbf{G}_r$. Note that in most cases $\mathbf{G}_r$ is real valued, so that $\overline{\mathbf{G}_r} = \mathbf{G}_r$):

$$\mathbf{z}_r = \mathcal{F}^{-1}\left(\overline{\mathbf{G}_r} \cdot \mathcal{F}(\mathbf{h}_r)\right) \tag{5}$$

All reconstructed channels are finally summed to obtain the reconstruction:

$$\mathcal{W}^\dagger(\mathbf{h}) = \sum_{r\in\Omega} \mathbf{z}_r = \mathcal{F}^{-1}\left(\sum_{r\in\Omega} \overline{\mathbf{G}_r} \cdot \mathcal{F}(\mathbf{h}_r)\right) \tag{6}$$

Because the image $\mathbf{x}$ is real, its Fourier transform has an hermitian symmetry. For this reason, we used band-pass Gabor filters covering only half of the Fourier plane, while the other half plane is further completed at the reconstruction using hermitian symmetry (this completion is obviated in the equations).

Because the transform is overcomplete, it can not be strictly bijective nor invertible because the transform domain has not the same dimension than the original domain. But, under the conditions that will be further exposed in Section II-H, $\mathcal{W}^\dagger$ can be the pseudo-inverse of $\mathcal{W}$ so that $\mathcal{W}^\dagger(\mathcal{W}(\mathbf{x})) = \mathbf{x},\ \forall \mathbf{x} \in \mathbb{R}^N$.

F. Downsampling

To limit the expansion of the transform domain it is desirable to downsample the channels as much as possible, but we desire to avoid at the same time any kind of aliasing. The *sparse downsampling* method [42] can be applied advantageously here for downsampling 3rd, 4th, 5th and low-pass filters both in u and v by factors of 2, 4, 8 and 8, respectively. The procedure is implemented in the Fourier domain as follows: a window of the defined downsampling size is centered on the filter and its position is adjusted so as to retain inside the maximum quantity of the filter amplitude (this operation is achieved by displacing iteratively the window in all the possible directions). Filter coefficients outside the window are then zeroed out. In this way, only filter coefficients smaller than 5% of the filter maximum are cut off which also preserves the smooth shape of the filters in the spatial domain. Using those filters, the channels can then be downsampled in an invertible manner without mixing frequencies (i.e. introducing aliasing): any frequency of the downsampled channel corresponds bijectively to one unique non-zeroed frequency in the upsampled version of the channel (see Fig. 6).

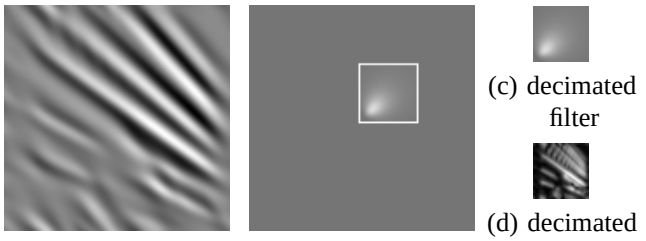

Fig. 6. Sparse downsampling method. **a.** 4th scale 2nd orientation channel of the image "MIT" (the original can be seen in Fig. 9). **b.** Corresponding log-Gabor filter (scale 4, orientation 2) represented in the Fourier domain (Fourier origin is situated in the center of the inset). A window of the desired downsampling size is adjusted on the filter so as to retain inside the maximum of the amplitude. Filters coefficients outside the window are zeroed out (only coefficients lower than 5% of the filter maximum are eliminated). **c.** The filter can be downsampled in an invertible manner by a factor 4×4 by eliminating the zero coefficients. **d.** The resulting downsampled channel after inverse Fourier transform has complex values.

The log-Gabor filters in quadrature of phase (i.e. complex-valued in the spatial domain) bring then an additional advantage: the filters lie only in one side of the Fourier domain allowing the implementation of the sparse downsampling method, while pure real or pure imaginary spatial filters are symmetric or antisymmetric in Fourier and compel to downsample in each dimension at Nyquist frequency, that is twice the highest frequency. This compensate largely that two real values (or a complex one) are obtained for each coefficient: complex-valued log-Gabor wavelets can still be downsampled by a factor around two times larger without aliasing. Consequently, the overcompleteness measured as the ratio M/N, where M is the dimension of the transform

domain and N is the dimension of the image, is reduced to a factor of 40 (it can be approximated as $\frac{14}{3}n_t$ where n_t is the number of orientations).

In parallel it is straightforward to demonstrate that exact reconstruction using the same non-orthogonal filters both for decomposition and reconstruction requires the transform to be overcomplete. And to preserve the smooth shape of the filters, M must be several times larger than N, here a higher downsampling would distort the filters. The overcomplete factor of 40 is then necessary. It is also consistent with the redundant number of simple cortical cells compared with the number of photoreceptor neurons [39] which can been evaluated as around 25.

The lack of aliasing guaranties the *shiftability* in space [1] (or translation invariance) which is of special importance for image processing tasks such as image denoising, image fusion, edge extraction, etc: the transform coefficients do not change drastically for a small displacement in space.

G. Matrix notation

Because the transform is linear, it can also be viewed as a matrix operation $W \in \mathbb{R}^{N\times M}$. $\mathcal{W}$ can then be described as the scalar product of $\mathbf{x} \in \mathbb{R}^N$ with a family of decomposition functions $(\mathbf{g}_k)_{k\in\{1,..,M\}}$ (the spatial log-Gabor functions), with each $\mathbf{g}_k \in \mathbb{R}^N$:

$$W\mathbf{x} = \mathbf{h} = (h_k)_{k\in\{1,..,M\}} = (< \mathbf{g}_k, \mathbf{x} >)_{k\in\{1,..,M\}} \quad (7)$$

Because we use the same filters $\mathbf{g}_k$ for reconstruction, the inverse transform is W^T (where ^{T} refers to the transposed matrix) and for all $\mathbf{h} \in \mathbb{R}^M$:

$$W^T\mathbf{h} = \sum_{k=1}^{M} h_k\mathbf{g}_k \quad (8)$$

Under the conditions defined in Section II-H, W^T provides exact reconstruction. Thus the transform is said *self-invertible* (i.e. exact reconstruction is achieved using the same filters both for the decomposition and the reconstruction) [1].

H. Methods for reconstruction improvement and exact reconstruction

The condition of exact reconstruction comes from Eq. 3 and Eq. 6 as:

$$\sum_{r\in\Omega} |\mathbf{G}_r|^2 = 1 \quad (9)$$

In the sequel we propose different methods for improving the reconstruction, i.e. making $\sum_{r\in\Omega} |\mathbf{G}_r|^2$ closer to 1.

1) Hexagonal Fourier lattice by shifting even scales in orientation: As already included in Eq. 1 in the definition of $\theta_{(s,t)}$, every second scale is shifted in orientation by $\frac{1}{2}\frac{\pi}{n_t}$ angle. This shift induces a hexagonal configuration which provides a more uniform coverage of the Fourier domain [2] (see also Fig 1.a).

2) Bandwidth adjustment: The bandwidths defined by Eq. 1 have been empirically adjusted and allow a fairly uniform coverage of the Fourier domain with variation $\sum |\mathbf{G}_r|^2$ lower than 0.6% between the 2nd and 5th scale.

3) Exact reconstruction: Each filter $\mathbf{G}_r(u,v)$ is finally normalized by $\sqrt{\sum_{r\in\Omega} |\mathbf{G}_r|^2(u,v)}$, thus from Eq. 9 we have exact reconstruction filters. Because the filters are already very close to the flat response before the division, the deformation introduced is small (maximum 0.6% between the 2nd and 5th scale) and does not produce important distortions in the spatial domain (e.g. sides lobes are very small in amplitude). We have now $\forall \mathbf{x} \in \mathbb{R}^N,\ W^TW\mathbf{x} = \mathbf{x}$. Note nevertheless that, due to the overcompleteness, in general $WW^T\mathbf{h}$ is not equal to $\mathbf{h}$: $\exists \mathbf{h} \in \mathbb{R}^M,\ WW^T\mathbf{h} \neq \mathbf{h}$.

III. Application to Image denoising

The present log-Gabor wavelet scheme has already be shown efficient in many classical image processing applications such as edge extraction [33], [34], image fusion [37], image denoising [33], [34] and also image compression [35], [36], [43]. Here to illustrate the efficiency of the transform we propose to compare its ability to segregate the noise from the signal in an image denoising scenario.

Most currently used denoising methods are based on anisotropic diffusion [44], [45], [46] or wavelet thresholding [26], [27], [28], [30]. Wavelet or multiresolution image denoising applications usually proceed in three stages, first a transformation, then a thresholding operation and finally the inverse transform for reconstructing the image. The transform aims at describing the signal in a domain where image contains (principally the contrast edges) have statistically different amplitude than the noise: edges induce high amplitude coefficients while spatially incoherent noise produces a low level of amplitude spread in all the coefficients. A basic thresholding permits then to segregate most of the signal from the noise. There exist many methods for determining the optimal threshold [26], [20], [47], [28] (see [48] for a review). Moreover more elaborated methods [49], [30] also uses the context (i.e. they take into account the neighborhood of each coefficient instead of solely the coefficient in order to decide if it is signal or noise). It is also to note that the thresholding operation has a biological justification [50].

Here we aim at comparing only the efficiency of the log-Gabor wavelets transform in comparison with other transforms independently of the method for threshold determination. Therefore we will test the transform in a series of images - where Gaussian noise has been added- by applying a gradient descent technique for finding the best threshold, i.e. the one giving the highest PSNR (Peak Signal-to-Noise Ratio) to the given original image. Thus, the experiment finds the best result achievable if the threshold determination technique would be optimal. It measures then the ability of each transform to separate the signal from the noise by thresholding. Note that these experiments are not only significant for image denoising since the possibility to code the image content through a reduced set of large coefficients is of primary importance in many classical image processing tasks (coding, denoising, edge extraction...).

In all the experiments and for all the transform-based methods tested five scales will be used. A threshold is determined for each scale by gradient descent searching for the best PSNR

to the original image. No strategy has been employed for improving the response close to the borders of the image in any method. This allows to visualize the artifacts (e.g. ringing) due to the abrupt edges in those regions.

A. Number of orientations

The first experiment aims at determining the optimal number of orientations to be used with log-Gabor wavelets. The question of the number of orientations is important since bi-orthogonal wavelets deploy just 3 orientations whereas more recent studies claimed the necessity of 6 orientations [4], [5], 8 orientations or more [30], [33], a variable number of orientations depending of the scale [8], or even up to 64 orientations [7].

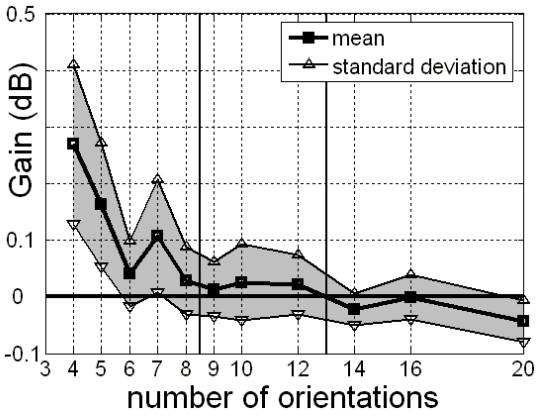

Fig. 7. Denoising results as a function of the number of orientations. The denoising results are calculated over a set of 6 images (the same as in Table I), each of them tested with 3 different levels of noise (the PSNR is around 14, 20 and 28 dB). To reduce the influence of the large variability of conditions across experiments, the mean and standard deviation (in dB) are calculated taking as reference the previous number of orientation tested. Results show then how the denoising improves when the number of orientations is incremented from 3 to 4 orientations, from 4 to 5, etc. Results improve clearly from 3 to 8 orientations, they then achieve a maximum around 12 orientations and latter decrease slowly when more orientations are employed (see also the filter shapes as a function of the number of orientations in Fig. 1.d).

Results gathered in Fig. 7 show that: the denoising improves importantly between 3 and 8 orientations which confirms the necessity of using more orientations than bi-orthogonal wavelets do; the better results are obtained around 8 or 12 orientations but with variability, since in particular cases the best results are obtained with as few as 5 or 6 orientations or as many as 16 or 20 orientations. Visually (see Fig. 8) 12 or 16 orientations yield artificial looking elongated artifacts. Such effect does not appear, or at least is much less salient when using 8 orientations.

These results support the choice of 8 orientations as a compromise between a low mathematical error and a good perceptual quality. This choice is also consistent with biological models of simple cells described in Section II-A. Moreover it will allow to fairly compare with the steerable pyramids used in [30], since they also implement 8 orientations.

Note also that in our scheme (as in other studies, see e.g. [7], [8]) the bandwidth varies depending on the number of orientations. Nevertheless it would be interesting to test both the number of orientations and the bandwidth parameters separately.

B. Comparison between multiresolution transforms

In Table I log-Gabor wavelets with 8 orientations are compared with bi-orthogonal wavelets 'Db4' [26], undecimated wavelets 'Db4' [27], [28], [29], and steerable pyramids with 8 orientations [30], [1] (see the shape of the filters Fig. 1). *Soft thresholding* is applied in the first two methods. It consists in zeroing all coefficients which amplitude is below a threshold and the diminishing (or *shrinkage*) by the threshold value of the amplitude of the other coefficients. We verified that for almost all the experiments soft thresholding provides better results than *hard thresholding* (zeroing of the coefficients below a threshold) for critically sampled wavelets and also, although in a lower amount, for undecimated wavelets. On the contrary hard thresholding yields better results for steerable pyramids and log-Gabor wavelets (data not shown). Hard thresholding is then used for both those methods. For log-Gabor wavelets the threshold is applied in the modulus of the complex coefficients with exception of the first scale where it is applied separately on the real and imaginary parts of the coefficients because they do not correspond to the same position (see section II-B). It is not totally surprising that hard thresholding performs better that soft thresholding since it preserves better the high amplitude coefficients. On the contrary the fact that soft thresholding provides better results for biorthogonal wavelets could be due in part to the lack of translation invariance (that would explain soft thresholding does not improve so much the results of undecimated wavelets) and perhaps also to the lower degree matching between decomposition functions and image features.

It appears from Table I that apart from very few exceptions, undecimated wavelets always provide better results than critically sampled wavelets (+0.51 dB of improvement in mean, the standard deviation being σ=0.18 dB). Steerable pyramids provide better results than undecimated wavelets (+0.40$\pm$0.36 dB of improvement) and log-Gabor wavelets outperform all the former three methods (+0.38$\pm$0.26 dB of improvement compared with steerable pyramids, PSNR improvements being observed in each of the 30 cases tested). In each method the denoised images still contains small quantities of artifacts due to noise. Visual inspection on the Fig. 9 and 10 lets see that the shape of the artefacts corresponds to the shape of the decomposition functions shown Fig. 1. The quantity of noise features could be reduced by a more severe thresholding and here a significant quantity of noise feature remains because the thresholds are adjusted for the best PSNR. The thresholding should be a bit higher for avoiding most of the artifacts at the cost of loosing an additional part of the signal. This would be perceptually more pleasant even if the PSNR would be worst. It is remarkable that the log-Gabor method generally induces less amount of artifacts (particularly when compared with biorthogonal and undecimated wavelets but also in comparison with steerable pyramids) which would indicate an augmented ability for edge to noise segregation. In addition the artifacts appear more natural looking and are less annoying so that they

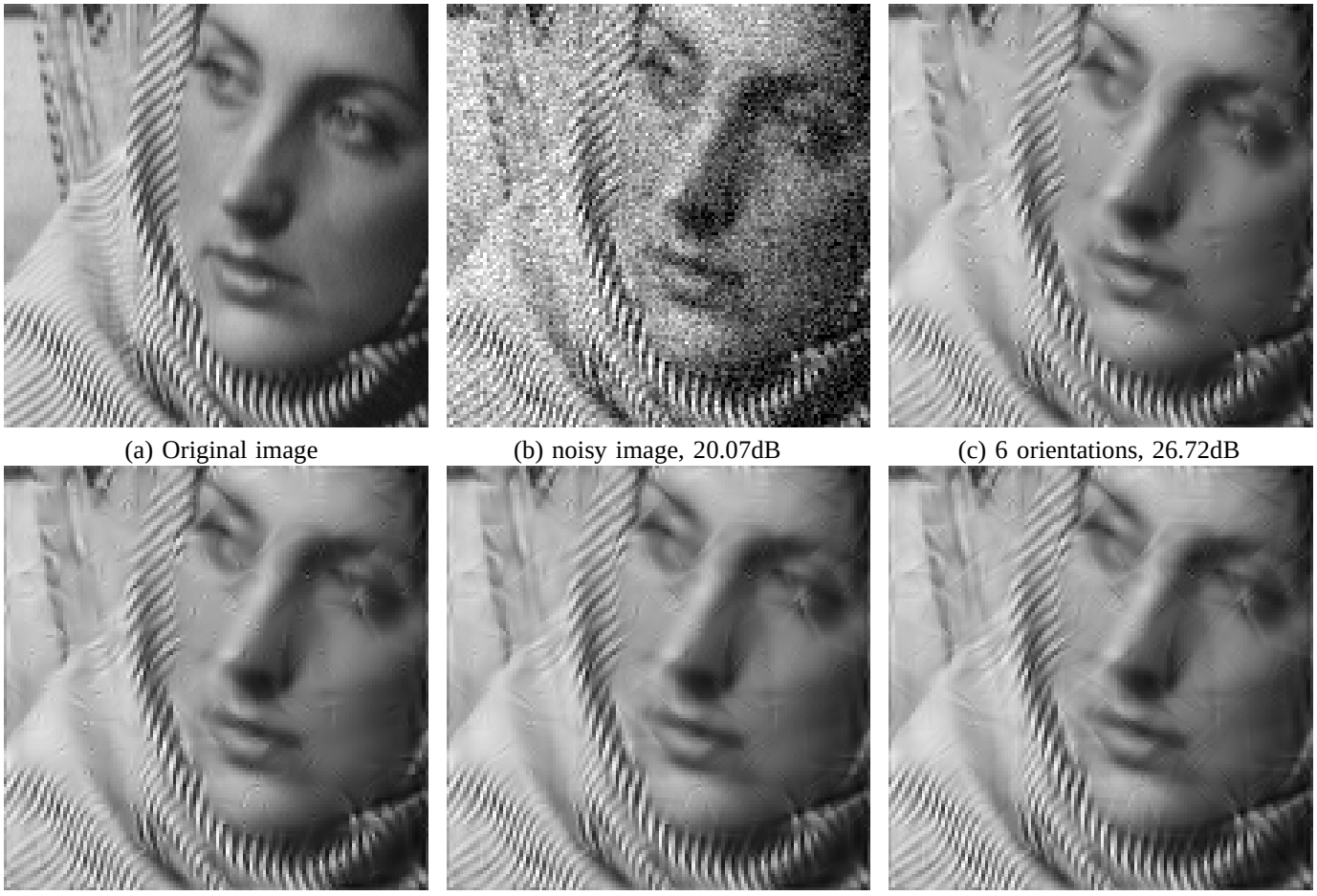

(a) Original image (b) noisy image, 20.07dB (c) 6 orientations, 26.72dB

(d) 8 orientations, 26.82dB (d) 12 orientations, 27.10dB (f) 16 orientations, 27.10dB

Fig. 8. Denoising results through log-Gabor wavelets using different number of orientations. **a.** 128×128 detail of the image "Barbara". **b.** The noisy image has a PSNR equal to 20.07dB. **c.** In the denoising using 6 orientations an significant quantity of high amplitude noise points are still visible. The small size of the filters could explain the lower segregation between edges and noise. **d.** Using 8 orientations, the number of noise points is reduced. **e.** Using 12 orientations, almost all isolated noise points are removed but some elongated artifacts appear. **f.** Although the best PSNR result is obtained for 16 orientations, the scheme produces many salient elongated artifacts.

can even be confounded with the signal (specially for non-human images, see Fig. 9). It has already been established that the translation invariance property improves the results of over-complete representations in comparison to critically sampled ones [1], [27], [28], [29], also because of the aliasing present in critically sampled wavelets. The use of more orientations can explain the better results of steerable pyramids and log-Gabor wavelets on undecimated wavelets. Note moreover that the finer bandwidth in orientation yields larger filters in the space domain then involves more pixels in the calculation of the coefficients: the noise is averaged on more pixels what leads a better noise robustness (Fig. 1.d shows how the filter size increases with the number of orientations).

The better performances of the log-Gabor representation in comparison to steerable pyramids could be explained by four factors: (1) the Gabor (Gaussian) filter's shape offers the optimum joint localization in frequency and space, which is an improvement in comparison with the raised cosine shape of steerable pyramids. (2) Log-Gabor functions are complex-valued with odd and even parts which permits a better capture of edges and ridges [20], [33]. (3) The oriented high-pass log-Gabor filters are smooth and without extra side-lobe in space (while the high-pass of steerable pyramids [30] shown in Fig. 1.f seem to be constructed without all the precautions described in section II-B). (4) The proposed log-Gabor filters have elongated shape whereas steerable filters are more isotropic in size, i.e. log-Gabor have larger bandwidth in frequency (1.43 octave against 1 octave for steerable pyramids) and narrower bandwidth in orientation (37 degrees against 50 degrees for steerable). The elongated shape seems more appropriate for two reasons: they are adapted from biological data and they are also closer to the independent component of the natural images extracted by sparse coding or ICA techniques [31], [32]. Thus the log-Gabor functions should match better with edges of natural images (yielding a stronger differential response in edge vs. noise features) and as an additional advantage they could appear more natural looking to human observers.

IV. Conclusions

We proposed an overcomplete multiresolution scheme mimicking the receptive field properties of simple cortical cells and

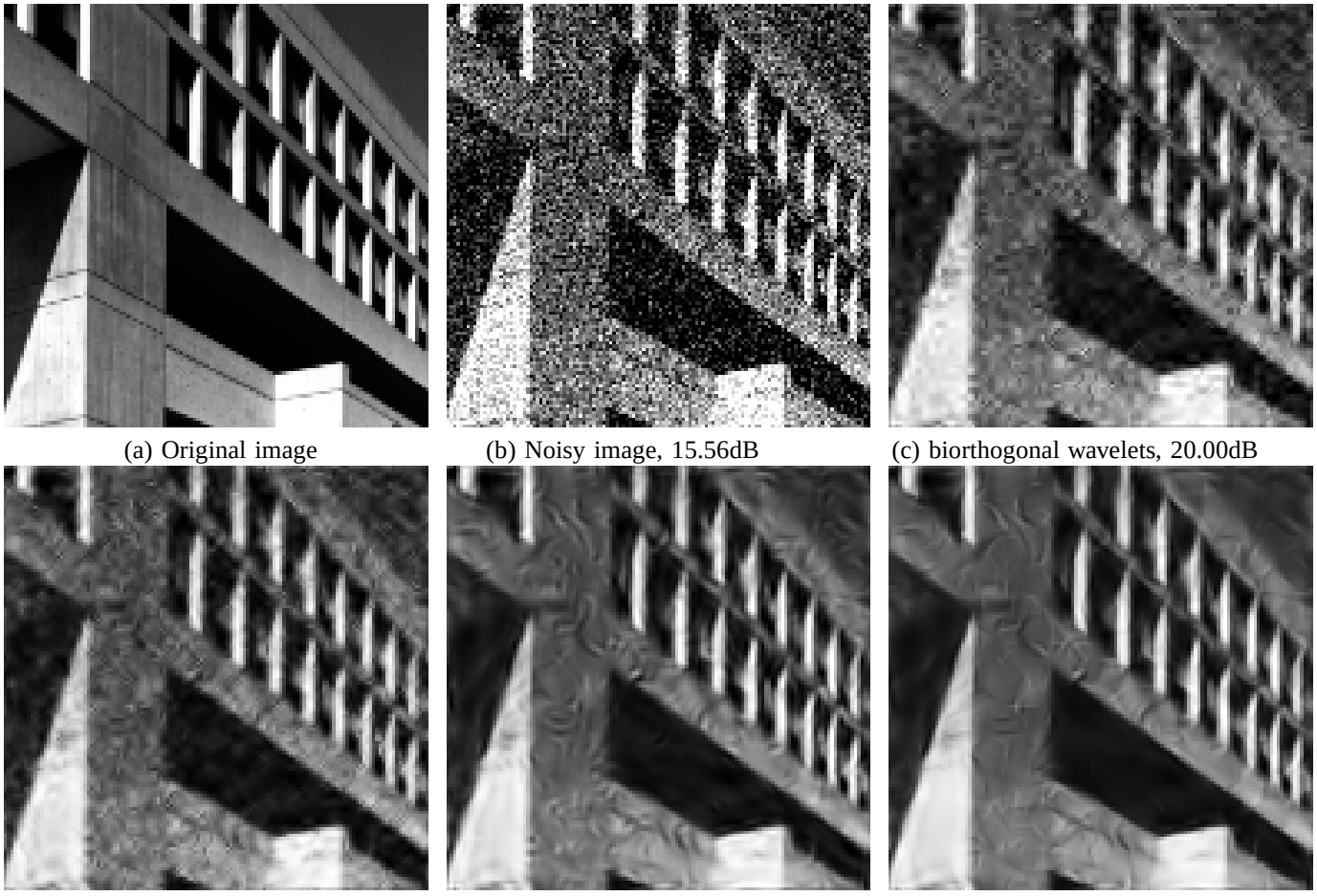

(a) Original image (b) Noisy image, 15.56dB (c) biorthogonal wavelets, 20.00dB

(d) undecimated wavelets, 20.57dB (e) Steerable pyramid, 21.25dB (f) log-Gabor wavelets, 21.77dB

Fig. 9. Denoising results. **a.** 128×128 pixel detail of the image "MIT". **b.** The noisy version has a PSNR of 15.56dB. **c.** Denoising by wavelets provides a 20.00dB denoised image. **d.** Undecimated wavelets yield a 20.57dB denoised image. **e.** Steerable pyramid yields a 21.25dB denoised image. **f.** Log-Gabor wavelets achieve a 21.77dB denoised image. The quantity of artifacts gets lower from (c) to (f). Moreover the ones appearing through log-Gabor wavelets denoising appear more natural-looking, and could in some cases even be confounded with image features.

optimized for achieving exact reconstruction through carefully designed filters. The proposed log-Gabor wavelet transform is interesting in several aspects. First from the mathematical point of view, since Gabor functions are optimally joint-localized in frequency and space, which makes them optimal functions to characterize signals, and also because the transform is self-invertible which has been shown important for preventing the appearance of artifacts. Second for biological reasons, since the transform filters mimic closely the receptive field of V1 simple cortical cells. The proximity to biological vision can help simultaneously for choosing adequate transform parameters, for limiting the saliency of the artifacts and for further developing the biological models. And third, in relation with statistics of natural images, since the transform filters have similar shape as the independent components learned from natural images, which support the proposed log-Gabor wavelets as an adequate scheme for matching natural image features. The transform showed excellent results for segregating the signal from the noise by hard thresholding. The comparison with other methods (bi-orthogonal wavelets, undecimated wavelets and steerable pyramids) showed an overall better performance of the proposed log-Gabor wavelets technique. The transform confirms then to be an adequate tool for representing features of natural images and to segregate them from the noise.

As further works, a whole image denoising application could be set up by implemented a dedicated threshold determination which took into account the relationships between neighboring coefficients as proposed e.g. in [49], [30]. Many other applications can also be derived since the ability of coding image features through a reduced set of large transform coefficients makes the transformation suitable for many applications such as image fusion or feature extraction. For image compression but also for general applications the redundancy induced by the overcompleteness could be recovered by deploying sparse coding algorithms [51], [36].

REFERENCES

[1] E.P. Simoncelli, W.T. Freeman, and D. J. Heeger, "Shiftable multiscale transforms," *IEEE Trans. Inf. Theory*, vol. 38, no. 2, pp. 587–607, 1992.

[2] M.H. Gross and R. Koch, "Visualization of multidimensional shape and texture features in laser range data using complex-valued Gabor wavelets," *IEEE Trans. Visual. and Comput. Graphics*, vol. 1, no. 1, pp. 44–59, 1995.

(a) Original image (b) Noisy image, 20.34dB (c) biorthogonal wavelets, 24.37dB

(d) undecimated wavelets, 24.99dB (e) Steerable pyramid, 25.52dB (f) log-Gabor wavelets, 26.01dB

Fig. 10. Denoising results. **a.** 128×128 detail of the image "Lena". **b.** The noisy version has a PSNR equal to 20.34dB. **c.** Denoising by wavelets provides a 24.37dB denoised image. **d.** Undecimated wavelets yield a 24.99dB denoised image. **e.** Steerable pyramid yields a 25.52dB denoised image. **f.** Log-Gabor achieves a 26.01dB denoised image.

[3] O. Nestares, R. Navarro, J. Portilla, and A. Tabernero, "Efficient spatial-domain implementation of a multiscale image representation based on Gabor functions," *Jour. of Eletr. Imag.*, vol. 7, no. 1, pp. 166–173, 1998.

[4] Y.M. Ro, M. Kim, H. K. Kang, B.S. Manjunath, and J. Kim, "MPEG-7 homogeneous texture descriptor," *ETRI Journal*, vol. 23, no. 2, pp. 41–51, 2001.

[5] N.G. Kingsbury, "Complex wavelets for shift invariant analysis and filtering of signals," *Jour. of Applied and Comput. Harmonic Analysis*, vol. 10, no. 3, pp. 234–253, 2001.

[6] J. Portilla and E. P. Simoncelli, "A parametric texture model based on joint statistics of complex wavelet coefficients," *International Journal of Computer Vision*, vol. 40, no. 1, pp. 49–70, 2000.

[7] J. L. Starck, E. J. Candès, and D. L. Donoho, "The curvelet transform for image denoising," *IEEE Trans. on Image Proc.*, vol. 11, no. 6, pp. 670–684, 2002.

[8] M.N. Do and M. Vetterli, "The contourlet transform: An efficient directional multiresolution image representation," *IEEE Trans. on Image Proc.*, vol. 14, no. 12, pp. 2091–2106, 2005.

[9] D. Gabor, "Theory of Communication," *J. Inst. Electr. Eng.*, vol. 93, pp. 429–457, 1946.

[10] J. Daugman, "Uncertainty relation for resolution in space, spatial frequency, and orientation optimized by two-dimensional visual cortical filters," *J. Opt. Soc. Am. A*, vol. 2, no. 7, pp. 1160–1169, 1985.

[11] S. Marcelja, "Mathematical description of the responses of simple cortical cells," *J. Opt. Soc. Am. A*, vol. 70, no. 11, pp. 1297–1300, 1980.

[12] D.A. Clausi and M.E. Jernigan, "Designing Gabor filters for optimal texture separability," *Pattern Recognition*, vol. 33, pp. 1835–1849, 2000.

[13] J. Portilla, R. Navarro, O. Nestares, and A. Tabernero, "Texture synthesis-by-analysis based on a multiscale early-vision model," *Opt. Eng.*, vol. 35, no. 8, pp. 1–15, 1996.

[14] F. Heitger, R. Von der Heydt, E. Peterhans, L. Rosenthaler, and O. Kubler, "Simulation of neural contour mechanisms: representing anomalous contours," *Image and Vision Computing*, vol. 16, pp. 409–423, 1998.

[15] P. Kovesi, "Phase congruency detects corners and edges," in *Australian Pattern Recog. Soc. Conf. DICTA'03. Sydney WA.*, 2003, pp. 309–318.

[16] C. Grigorescu, N. Petkov, and M. A. Westenberg, "Contour detection based on nonclassical receptive field inhibition," *IEEE Trans. on Image Proc.*, vol. 12, no. 7, pp. 729–739, 2003.

[17] M. Pötzsch, N. Krüger, and C. Malsburg, "Improving object recognition by transforming Gabor filter responses," *Network: Computation in Neural Systems*, vol. 7, no. 2, pp. 341–347, 1996.

[18] V. Krüger, *Gabor wavelet networks for object representation*, Ph.D. thesis, Christian-Albrechts-University Kiel, Technical Faculty, 2001.

[19] G. Cristóbal and R. Navarro, "Space and frequency variant image enhancement based on a Gabor representation," *Patt. Rec. Letters*, vol. 15, no. 3, pp. 273–277, 1994.

[20] P. Kovesi, "Phase preserving denoising of images," in *Australian Pattern Recog. Soc. Conf. DICTA'99. Perth WA.*, 1999, pp. 212–217.

[21] E. Mingolla, W. Ross, and S. Grossberg, "A neural network for enhancing boundaries and surfaces in synthetic aperture radar images," *Neural Networks*, vol. 12, no. 3, pp. 499 – 511, 1999.

[22] O. Christiansen, *Time-frequency analysis and its applications in denoising*, Ph.D. thesis, Dept. of Informatics, University of Bergen, Norway, 2002.

[23] D.J. Field, "Relation between the statistics of natural images and the response properties of cortical cells," *J. Opt. Soc. Am. A*, vol. 4, no. 12, pp. 2379–2394, 1987.

TABLE I

DENOISING RESULTS. RESULTS ARE GIVEN AS PEAK SIGNAL-TO-NOISE RATIO, $20log_{10}(1/\sigma_e)$ IN DB, WHERE σ_e IS THE ROOT MEAN SQUARE ERROR BETWEEN THE ORIGINAL AND THE DENOISED IMAGE. MEAN μ AND STANDARD DEVIATION σ ARE GIVEN IN EACH CASE IN COMPARISON WITH THE PREVIOUS METHOD.

Original image	noise level	biorthog. wavelets	undecimated wavelets	steerable pyramids	log-Gabor wavelets
barbara	34.10	35.42	35.88	36.54	**37.12**
	28.11	30.36	30.99	32.16	**32.57**
	20.25	24.6	25.27	26.70	**26.72**
	14.74	21.08	21.64	22.69	**22.92**
	10.25	18.52	18.82	19.14	**19.28**
teapot	34.33	35.28	35.83	36.01	**36.45**
	28.41	30.12	30.90	31.24	**31.63**
	20.71	24.44	25.28	25.62	**25.79**
	15.06	20.75	21.45	21.69	**21.77**
	10.41	17.48	17.91	17.96	**18.06**
mandrill	34.12	34.29	**34.35**	34.30	**34.35**
	28.09	28.65	28.83	28.96	**29.06**
	20.3	22.24	22.77	23.26	**23.42**
	14.75	18.64	19.25	19.73	**20.01**
	10.28	16.22	16.67	16.98	**17.16**
house	34.15	35.66	36.13	36.09	**36.52**
	28.2	31.31	32.02	32.36	**32.94**
	20.38	26.86	27.59	28.28	**29.10**
	14.78	23.58	24.09	24.83	**25.37**
	10.2	19.94	20.27	20.72	**20.89**
lena	33.97	34.83	35.10	35.01	**35.45**
	28.15	29.79	30.23	30.54	**31.11**
	20.34	24.37	24.99	25.52	**26.01**
	14.89	21.27	21.80	22.16	**22.59**
	10.26	18.32	18.67	18.78	**18.94**
mit	34.82	35.73	36.12	36.06	**36.94**
	28.79	30.51	31.10	31.22	**32.29**
	20.98	24.10	24.85	25.29	**25.95**
	15.56	20.00	20.57	21.25	**21.77**
	10.64	16.21	16.56	16.86	**17.10**
mean improvement (μ,σ)	34	+0.95 $\pm$0.42	+0.37 $\pm$0.16	+0.10 $\pm$0.26	+0.47 $\pm$ 0.25
	28	+1.83 $\pm$0.76	+0.55 $\pm$0.20	+0.40 $\pm$0.35	+0.52 $\pm$ 0.29
	20	+3.94 $\pm$1.38	+0.69 $\pm$0.096	+0.65 $\pm$0.36	+0.39 $\pm$ 0.29
	15	+5.92 $\pm$1.58	+0.58 $\pm$0.062	+0.59 $\pm$0.27	+0.35 $\pm$ 0.16
	10	+7.44 $\pm$1.43	+0.37 $\pm$0.053	+0.26 $\pm$0.14	+0.16 $\pm$ 0.044
	all level	+4.02 $\pm$2.71	+0.511 $\pm$0.180	+0.402 $\pm$0.355	+0.378 $\pm$ 0.259

[24] J. Daugman, "Complete discrete 2-D Gabor transforms by neural networks for image analysis and compression," *IEEE Trans. Acoust. Speech Signal Proc.*, vol. 36, no. 7, pp. 1169–1179, 1988.

[25] T.S. Lee, "Image representation using 2D Gabor wavelets," *IEEE Trans. Pattern Anal. Mach. Intell.*, vol. 18, no. 10, pp. 959–971, 1996.

[26] D. Donoho, "De-noising by soft-thresholding," *IEEE Trans. Inf. Theory*, vol. 41, no. 3, pp. 613–627, 1995.

[27] R.R. Coifman and D. Donoho, "Translation-invariant de-noising," in *Wavelets and statistics, Lecture Notes in Statistics 103*, A. Antoniadis and G. Oppenheim, Eds., pp. 125–150. Springer Verlag, New York, NY, 1995.

[28] S. G. Chang, B. Yu, and M. Vetterli, "Adaptive wavelet thresholding for image denoising and compression," *IEEE Trans. on Image Proc.*, vol. 9, no. 9, pp. 1532–1546, 2000.

[29] X. Li and M.T. Orchard, "Spatially adaptive image denoising under overcomplete expansion," in *Int. Conf. on Image Proc.*, 2000, vol. 3, pp. 300–303.

[30] J. Portilla, V. Strela, M. Wainwright, and E. Simoncelli, "Image denoising using scale mixtures of Gaussians in the wavelet domain," *IEEE Trans. Image Proc.*, vol. 12, no. 11, pp. 1338–1351, 2003.

[31] B. Olshausen and D.J. Field, "Wavelet-like receptive fields emerge from a network that learns sparse codes for natural images," *Nature*, vol. 381, pp. 607–609, 1996.

[32] E. Doi and M. S Lewicki, "Relations between the statistical regularities of natural images and the response properties of the early visual system," *Japanese Cognitive Science Society, SIG P&P*, pp. 1–8, 2005.

[33] S. Fischer, R. Redondo, L. Perrinet, and G. Cristóbal, "Sparse Gabor wavelets by local operations," in *Proc. SPIE, Bioengineered and Bioinspired Systems II*, Gustavo Linan-Cembrano; Ricardo A. Carmona, Ed., Jun 2005, vol. 5839, pp. 75–86.

[34] R. Redondo, S. Fischer, L. Perrinet, and G. Cristóbal, "Modeling of simple cells through a sparse overcomplete Gabor wavelet representation based on local inhibition and facilitation," in *European Conf. On Visual Perception, A Coruña, Spain*, august 2005.

[35] S. Fischer, G. Cristóbal, and R. Redondo, "Sparse overcomplete Gabor wavelet representation based on local competitions," *IEEE Trans. on Image Proc.*, vol. 15, no. 2, pp. 265–272, 2006.

[36] S. Fischer, R. Redondo, and G. Cristóbal, "Sparse edge coding using overcomplete Gabor wavelets," in *IEEE Int. Conf. on Image Proc., Genova*, 2005, vol. 1, pp. 85–88.

[37] R. Redondo, F. Sroubek, S. Fischer, and G. Cristóbal, "A multiresolution-based fusion scheme through log-Gabor wavelets and a multisize windows technique," *Information Fusion*, submitted.

[38] D.A. Pollen and S.F. Ronner, "Phase relationships between adjacent simple cells in the visual cortex," *Science*, vol. 212, pp. 1409–1411, 1981.

[39] D. Hubel, *Eye, Brain, and Vision*, WH Freeman. Scientific American Library Series, New York, 1988.

[40] R. L. DeValois, D. G. Albrecht, and L. G. Thorell, "Spatial frequency selectivity of cells in macaque visual cortex," *Vision Res.*, vol. 22, pp. 545–559, 1982.

[41] J. Morlet, G. Arens, E. Fourgeau, and D. Girard, "Wave propagation and sampling theory," *Geophysics*, vol. 47, pp. 203–236, 1982.

[42] R. Wurtz, *Multilayer dynamic link networks for establishing image point correspondences and visual object recognition*, Ph.D. thesis, Bochum University, 1994.

[43] S. Fischer, R. Redondo, L. Perrinet, and G. Cristóbal, "Sparse coding of images inspired by the functional architecture of the primary visual areas," *EURASIP JASP, special issue on Image Perception*, submitted.

[44] D. Tschumperlé and R. Deriche, "Vector-valued image regularization with PDE's : A common framework for different applications," *IEEE Trans. on Pattern Analysis and Machine Intelligence*, vol. 27, no. 4, pp. 506–517, 2005.

[45] F. Sroubek and J. Flusser, "Multichannel blind iterative image restoration," *IEEE Trans. Image Proc.*, vol. 12, no. 9, pp. 1094–1106, 2003.

[46] A. B. Hamza, H. Krim, and G. Unal, "Unifying probabilistic and variational estimation," *IEEE Signal Proc.*, vol. 19, no. 5, pp. 37–47, 2002.

[47] S. Zhong and V. Cherkassky, "Image denoising using wavelet thresholding and model selection," in *Int. Conf. on Image Proc.*, 2000, vol. 3, pp. 262–265.

[48] C. Taswell, "The what, how and why of wavelet shrinkage denoising," *Computing in Science and Engineering*, pp. 12–19, 2000.

[49] S. G. Chang, B. Yu, and M. Vetterli, "Spatially adaptive wavelet thresholding with context modeling for image denoising," *IEEE Trans. on Image Processing*, vol. 9, no. 9, pp. 1522–1531, 2000.

[50] L. Perrinet, M. Samuelides, and S. Thorpe, "Coding static natural images using spiking event times: do neurons cooperate?," *IEEE Trans. on Neural Networks*, vol. 15, no. 5, pp. 1164–75, 2004.

[51] L. Perrinet, "Feature detection using spikes : the greedy approach.," *Journal of Physiology (Paris)*, vol. 98, no. 4-6, pp. 530–9, July-November 2004.